Quantum coherence effects in quasidegenerate two-level atomic systems

Yabin Dong, Haihong Wang, Jiangrui Gao, and Junxiang Zhang*
State Key Laboratory of Quantum Optics and Quantum Optics Devices, Institute of Opto-Electronics, Shanxi University, Taiyuan 030006, People's Republic of China
(Received 11 April 2006; published 12 December 2006)

The wealth of quantum coherence effects depending on the orientation of external magnetic field, the polarization of coupling and probe lights, and the Rabi frequency of the coupling beam are studied in transition $F_e=2\leftrightarrow F_g=3$ of Cs D_2 line. The split of electromagnetically induced transparency (EIT) resonances on two or three resonances determined by the different combination of the polarization of interaction lights and the direction of applied magnetic fields is obtained. The shifting and widening of the EIT resonances with the strength of the magnetic field (i.e., Zeeman splitting in the upper and lower levels) and Rabi frequency of the coupling beam increasing are also discussed. It may develop into the potential application for tunable multichannel optical information storage. On the other hand, an explanation of observed asymmetry of spectra by laser frequency offset from the optical resonance is given with theoretical calculation, which is in good agreement with the experimental results.

DOI: 10.1103/PhysRevA.74.063810 PACS number(s): 42.50.Gy

I. INTRODUCTION

It is well known that quantum coherence and interference in an atomic system can lead to interesting and important phenomena such as electromagnetically induced transparency (EIT) [1–3], coherent population trapping (CPT) [4–7], lasing without inversion (LWI) [8,9], and electromagnetically induced absorption (EIA) [10–13]. Besides the fundamental interests, these phenomena have promising applications in the enhancement of the refractive index [14], the design of highly sensitive magnetometers[15], quantum-information processing [16], quantum switches [17], quantum interferometric optical lithography [18], and optical propagation with slow or negative group velocity [19,20]. All these coherence effects have been widely studied in the three-level atomic system [21,22,1]. However, in real atomic systems, the atomic states usually have complex structure with degenerate Zeeman sublevels which can lead to interesting variations of absorption induced by the competition between EIT and absorption effects due to the interplay between the dominance of Rabi frequency and Zeeman splitting.

Recently, quantum coherences in the degenerate atomic system have attracted great interests because it exhibits not only the CPT and EIT of the simple three-level system and Mollow absorption spectrum (MAS) of a pure two-level system, but also EIA in the absorption spectra. The quantum coherences in the degenerate two-level system were extensively studied both experimentally and theoretically in Akulshin's group [23–25]. It was demonstrated that the enhancement of absorption (EIA) can occur in the degenerate two-level system for a closed transition $F_g\leftrightarrow F_e=F_g+1$ with $F_g>0$ because of the spontaneous transfer of the atomic coherence (TOC), and the dependence of EIA on the field polarization was also discussed. Later Goren *et al.* [26] found that EIA can also occur in open systems when the coupling and probe beams have the same polarization rather than a different polarization as in the case of EIA-TOC, and they concluded that this effect resulted from the EIA-TOP [EIA due to the collision transfer of population (TOP)]. Furthermore, the experimental demonstration of EIA was reported in the degenerate two-level open system regardless of angular momentum [27].

With the theoretical and experimental investigations, more and more complex quantum coherence effects related to the interactions between multifield and multilevel systems in the two-level system were developed. The first report about the spectroscopic features of the coherence resonance in the degenerate two-level system showed that the absorption spectra were strongly dependent on the external magnetic field, optical fields polarization, light intensity, and atomic level characteristics [24,25], and the split of EIT resonances on two, three, or five resonances was also reported [10]. Later the experimental realization of Gaussian light pulse propagation from subluminal to superluminal based on the transformation from EIT to EIA was obtained in the transition ($6\,^2S_{1/2}$, $F_g=4\leftrightarrow 6\,^2P_{3/2}$, $F_e=5$) of Cs D_2 line [28]. The theoretical discussion on transitions $F_e=0\leftrightarrow F_g=1$, $F_e=1\leftrightarrow F_g=2$, and $F_e=1\leftrightarrow F_g=0$ [29–31], which is driven by π or $\sigma_\pm$ light and probed by transverse lights with two equal left-handed and right-handed circular polarization components $\sigma_\pm$, showed that the absorption conversion from EIT to EIA and the effects of widening and shifting of EIT windows were investigated. All these effects can be considered as a result of the superposition of pure two-level, simple three-level Λ-type and V-type subsystems induced by the Zeeman splittings. Thus for any transition $F_e\leftrightarrow F_g$ with different polarizations of coupling and probe beams, the quantum coherent effects would present various phenomena because different superposition of the simple energy level configurations are involved. Motivated by this, in this paper, we experimentally and theoretically investigate the quantum effects in the transition $F_e=2\leftrightarrow F_g=3$ of the D_2 line of the Cs ensemble with a different combination of the polarization of coupling and probe lights, which results in the different

*Email address: junxiang@sxu.edu.cn

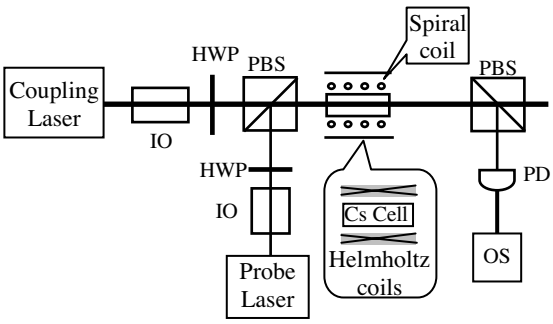

FIG. 1. The experimental arrangement. IO: isolator; HWP: half-wave plate; PBS: polarizing beam splitter; PD: photo detector; OS: oscilloscope.

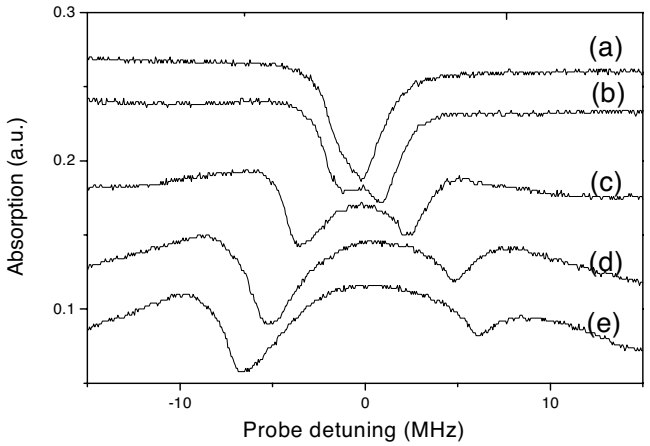

FIG. 2. The absorption spectra of the probe beam as a function of probe detuning with different magnetic field strength B. The intensity of the coupling and probe lights are $I_c=106.9$ mW/cm^2 and $I_p=9.6$ mW/cm^2. (a) EIT spectrum with the strength of magnetic field $B=0$ G. (b)–(e) Separated and shifted EIT peaks with $B=2.8$ G in curve (b); $B=8.4$ G in curve (c); $B=14$ G in curve (d); $B=19.6$ G in curve (e).

superposition of the V-type, Λ-type, and pure two-level subsystems; thus the absorption properties are greatly modified. In this system all of the pure two-level, V-type, and Λ-type three-level subsystems are involved in quantum coherence effects, we show that the number of EIT resonances is determined by a combination of the polarization of interaction lights and the direction of the magnetic fields as proved in Refs. [24,10]. The shifting of the EIT resonances is also obtained when we change the strength of the applied magnetic field. A qualitative agreement between experimental results and theoretical calculation is given by using the optical Bloch equation [29,32], especially the asymmetry of spectra is explained with this calculation. This effect might be developed in controllable propagation of more than one slow pulse light in one atomic system at the same time.

II. EXPERIMENTAL SETUP AND RESULTS

The experimental setup is shown in Fig. 1. Two diode-lasers (TOPTICA; DL100) with 700 kHz linewidth are used as coupling and probe lights. The frequency of the coupling beam is locked to the resonant transition between ground excited $F_e=2(6P_{3/2})$ and $F_g=3(6S_{1/2})$ levels using the standard technology of saturation absorption spectrum with a lock-in amplifier and a proportional and integrating amplifier. The frequency of the probe beam is scanned through the transition $F_e=2(6P_{3/2})\leftrightarrow F_g=3(6S_{2/1})$. At the same time, the frequencies of two lasers are monitored by Doppler-free saturated absorption spectroscopy. Both of the coupling and probe beams pass through an isolator to avoid the light feedback into the lasers, then after half-wave plates, the two beams with linearly polarizations are overlapped on a polarizing beam splitter before they are lead to the Cs vapor cell. The extinction ratios of the polarizing beam splitter is greater than 25 dB, thus the polarization of two beams are well linearly polarized and their polarizations are orthogonal to each other. The Cs cell is placed in a pair of Helmholtz coils at the side of the cell or a spiral coil to control the strength and direction of the magnetic field. A pair of coils is used to produce a weak magnetic field along the polarization direction of the coupling beam, and then the quantization axis of magnetic field is perpendicular to the polarization direction of the probe light. In this case, the coupling beam is treated as π polarization light, and meanwhile the probe light is treated as a transverse light with two equal left and right components $\sigma_{\pm}$. On the other hand, a spiral coil can produce longitudinal magnetic field (i.e., the quantization axis of magnetic field is perpendicular to the polarization of coupling and probe laser beams), thus both of the coupling and probe beams can be treated as transverse lights with two equal left-handed and right-handed circular polarization components $\sigma_{\pm}$. After passing through the Cs cell, the probe and coupling beams are separated with another polarizing beam splitter, the probe beam is detected by a photodiode and recorded by a digital oscilloscope. The spiral coil and the Cs vapor cell are shielded with μ metal sheets to avoid the magnetic field splitting of the sublevels from surrounding magnetic field.

Figure 2 shows the absorption spectra of the probe beam as a function of the probe detuning with different strength of magnetic field B when the atoms are put in a pair of Helmholtz coils, which give rise to a interaction configuration that the atoms are driven by a linearly polarized π light and probed by circularly polarized $\sigma_{\pm}$ lights. The total Rabi frequencies of the coupling and probe lights are fixed to be $\Omega_c=29.6$ MHz and $\Omega_p=8.9$ MHz, respectively, which is deduced from the definition about the Rabi frequency of light $\Omega=\Gamma\sqrt{I/2I_0}$; here Γ is the natural decay rate, $I=P/\pi r^2$ mW/cm^2 is power density of the field, and the saturation intensity is $I_0=1.65$ mW/cm^2. The corresponding powers of coupling and the probe beams are 106.9 mW/cm^2 and 9.6 mW/cm^2. From Figs. 2(a)–2(f), the strength of the magnetic field produced by a pair of Helmholtz coils is tuned from 0 G up to 19.6 G.

As shown in Fig. 2(a), the absorption of probe laser shows that the EIT effect is observed for a two-level system. If a magnetic field is applied, the degeneracy of both the excited and ground levels is broken, and the Zeeman sublevels appear. The involved multilevel coherence modifies the properties of probe absorption. It is seen from Fig. 2(b) that the

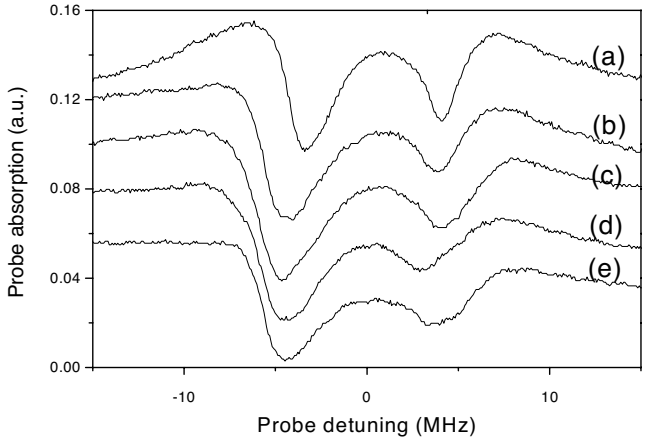

FIG. 3. The absorption spectra depending on the intensity of the coupling beam. The strength of magnetic field and probe beam are B=9.8 G and I_p=9.6 mW/cm^2. (a)–(f) The two EIT peaks become wider with the intensity of the coupling beam increasing. Curve (a) for I_c=393.6 mW/cm^2; curve (b) for I_c=296.2 mW/cm^2; curve (c) for I_c=203.8 mW/cm^2; curve (d) for I_c=106 mW/cm^2; curve (e) for I_c=43.6 mW/cm^2.

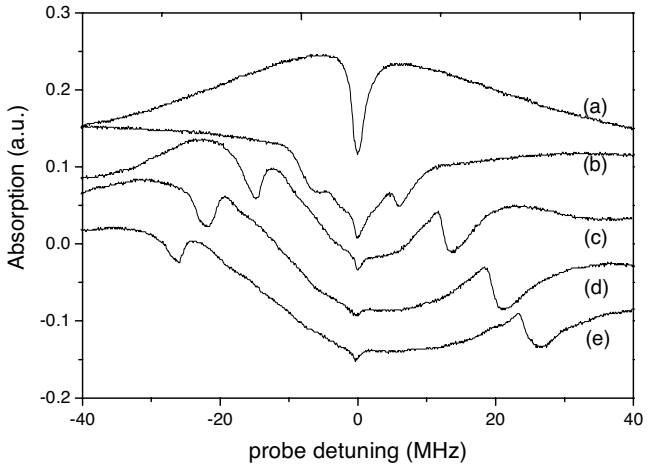

FIG. 4. The absorption spectra as a function of probe detuning for different intensity of magnetic field B. Here, I_c=83.1 mW/cm^2 and I_p=8.3 mW/cm^2. (a) EIT spectrum with the strength of magnetic field B=0 G. (b)–(g) the breaking up of the EIT peaks with B=4 G [curve (b)], B=8.8 G [curve (c)], B=13 G [curve (d)], B=17 G [curve (e)].

transparency peak begins to split. When the strength of magnetic field B is continuously increased, the EIT window breaks up into two peaks with a gap between them as shown in Fig. 2(c). When the strength of magnetic field B is further increased, the two peaks move apart from each other as seen in Fig. 2(d) and 2(e); and it is obviously seen that both the two transparency maxima shift their position away from the region of zero detuning with the strength of the magnetic field increasing.

Compared to the sub-MHz laser linewidth, the relatively broad EIT resonances are observed. It is worth mentioning that the EIT spectral line is controlled by the phase coherence of coupling and probe beam while the absolute laser linewidth is less important. To get a narrow EIT spectrum, some techniques has been used to generate mutually coherent laser fields, such as the laser frequency shifting with acousto-optical modulator as demonstrated in Refs. [10,24]. In our system, in order to obtain high power of the coupling beams, two independent extended cavity diode lasers are used, which is the main reason for the observed broadband EIT signals.

Figure 3 shows the absorption spectra for different intensity of the coupling beam when the strength of magnetic field B and probe beam are fixed. The strength of magnetic field B and the power of the probe beam are taken to be 9.8 G and 9.6 mW/cm^2. It is seen from Fig. 3(a)–3(f) that both the two EIT windows become narrower as the intensity of the coupling beam is decreased from 393.6 mW/cm^2 to 43.6 mW/cm^2, which corresponding to the Rabi frequency from 56.8 MHz to 18.9 MHz. The widening of the EIT windows at higher coupling intensity is most likely due to power broadening similar to the usual EIT case where the EIT linewidth is proportional to the intensity [33], the other reason may come from the effect of ac Stark shift on the quantum coherence, which is similar to the effect of the ac Stark shift on a quantum interference of general EIT [34].

On the other hand, when a spiral coil is applied instead of a pair of Helmholtz coils, the quantization axis of the magnetic field is perpendicular to both the polarization of coupling and probe laser beams, so that both of the linearly polarized coupling and probe lights are decomposed into a left-handed and right-handed circularly polarized component σ_+ and σ_-. In this case, the absorption spectra of the probe laser with a different strength of the magnetic field are shown in Fig. 4. The powers of coupling and probe beams are taken to be 83.1 mW/cm^2 and 8.3 mW/cm^2, respectively, the corresponding Rabi frequency are 26.1 MHz and 8.26 MHz. The intensity of the magnetic field B is increasing from 0 G [Fig. 4(a)] to 17 G [Fig. 4(e)]. Figure 4(a) is the absorption spectrum when the magnetic field of spiral coil is turned off, as expected for quantum coherence in the two-level system, the signal of probe beam after the Cs cell exhibits the typical EIT effect. We can see from Fig. 4(b) that the transparency peak is divided into three peaks when the magnetic field is applied. These three EIT peaks are separated and the two transparency peaks at both right and left sides are shifted, their position with the strength of magnetic field B increasing; on the contrary, the EIT peak in the center still keeps its position.

It can be seen from Fig. 4 that the spectra is different from that in Fig. 2, which rightly indicates that for the different scheme of the interaction, the quantum coherence presents different form, and the number of EIT resonances is determined by the combination of the polarization of interaction lights and the direction of applied magnetic fields. The detail discussion about it is given in the following theoretical analyses.

It is well know that EIT is one of the most important modern optical techniques that can be used for the implementation of information processing and storage [16]. Subsequent experimental works, such as transporting and time reversing light [35] and atomic memory for correlated photon states [36] via atomic coherence provided good

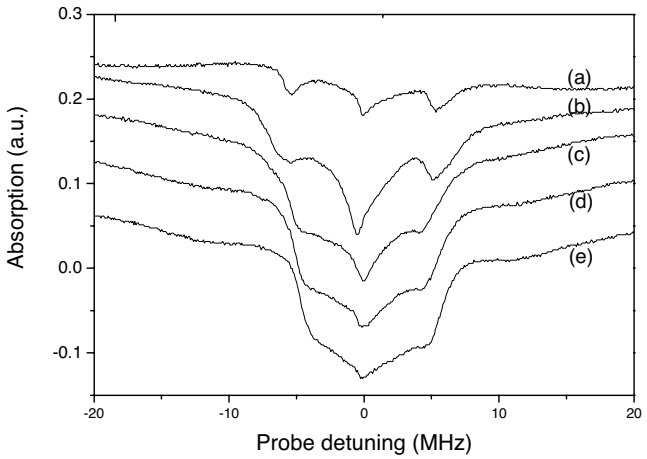

FIG. 5. Absorption spectra versus the detuning of probe beam for different intensity of the coupling beam. Here, $B=8.8$ G and $I_p=8.3$ mW/cm^2. Curve (a): $I_c=334.4$ mW/cm^2; curve (b): $I_c=258.2$ mW/cm^2; curve (c): $I_c=174.6$ mW/cm^2; curve (d): $I_c=88.6$ mW/cm^2; curve (e): $I_c=17.3$ mW/cm^2.

understanding of perspectives of its applications. The storing of a pair of pulses of light and dividing photon memory into two channels in four-level double-EIT systems have also been theoretically investigated [37,38]. In our system, it is possible to develop the multichannel information storage with the split EIT resonances in degenerate two-level systems.

The strength of magnetic field B and the power of probe beam are fixed to be 8 G and 8.3 mW/cm^2 (the Rabi frequency is 8.26 MHz), the absorption spectra depending on the different intensity of coupling beam are shown in Fig. 5. It is seen that all of the transparency peaks become narrower as shown in Figs. 5(a)–5(f) when the intensity of the coupling beam are decreased from 334.4 mW/cm^2 to 17.3 mW/cm^2 (the corresponding Rabi frequency is from 52.7 MHz to 11.9 MHz). For the large power of coupling beam, three EIT windows are almost overlapped because of the broadening effect as observed in Fig. 3, the reason for broadening is analyzed in the paragraph after Fig. 3. For this reason, the mediate power of the coupling beam should be chosen in real application.

It should be noted that the experimental results we obtained in Figs. 2–5 show that the transparency peaks are not symmetrical in their heights and positions as we have expected, which are proved to come from the effect of Doppler broadening. We theoretically analyze this effect by introducing a parameter in the term of laser detuning of coupling and probe beams, which explains the reason to break its symmetry. In the following section, we use the optical Bloch equations to qualitative explain the coherence effects we obtained for the real transition $F_e=2\leftrightarrow F_g=3$.

III. THE THEORETICAL ANALYSIS

Figure 6 shows the degenerate two-level system for transition $F_e=2\leftrightarrow F_g=3$. The Zeeman sublevels of excited states are expressed as $|e_{-2}\rangle$, $|e_{-1}\rangle$, $|e_0\rangle$, $|e_1\rangle$, and $|e_2\rangle$ for

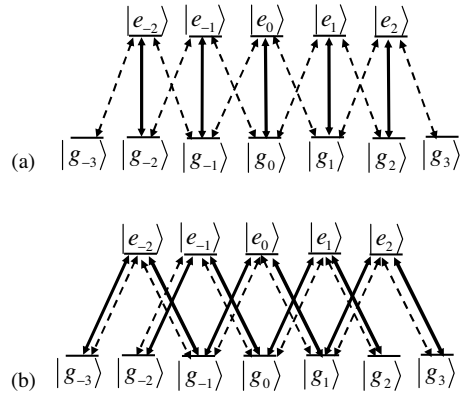

FIG. 6. Schematic energy level diagram for a transition $F_e=2\leftrightarrow F_g=3$. Solid lines represent the coupling light and dashed lines are for probe field. (a) The coupling and probe lights are linearly π and circularly $\sigma_\pm$ polarized respectively; (b) both of the coupling and probe lights are circularly $\sigma_\pm$ polarized.

$M_{F_e}=-2,-1,0,1,2$, while the ground states are $|g_{-3}\rangle$, $|g_{-2}\rangle$, $|g_{-1}\rangle$, $|g_0\rangle$, $|g_1\rangle$, $|g_2\rangle$, and $|g_3\rangle$ for $M_{F_g}=-3,-2,-1,0,1,2,3$. In the scheme of Fig. 6(a), the two-level system is driven by a linearly polarized π field with frequency ω_c and probed by circularly polarized $\sigma_\pm$ fields with frequency ω_p. The coupling beam with π polarization interacts with the transition $M_{F_e}=i\leftrightarrow M_{F_g}=i$ $(i=0,\pm1,\pm2)$, and meanwhile the $\sigma_\pm$ probe beams interact with the transition $M_{F_e}=i\leftrightarrow M_{F_g}=i\pm1$ $(i=0,\pm1,\pm2)$. Figure 6(b) is the configuration that both of the coupling and probe beams have two equal left-handed and right-handed circular polarized components $\sigma_\pm$. Here the lights with $\sigma_\pm$ polarization interact with the transition $M_{F_e}=i\leftrightarrow M_{F_g}=i\pm1$ $(i=0,\pm1,\pm2)$.

We write the evolution equations for the atomic variables as described in Refs. [26,29,39],

$$\dot{\rho}_{e_ig_j}=\frac{i}{\hbar}\left[\sum_k\left(V_{e_1g_k}\rho_{g_kg_j}-\rho_{e_ie_k}V_{e_kg_j}\right)\right]-(i\omega_{e_ig_j}+\Gamma_{e_ig_j})\rho_{e_ig_j}, \tag{1}$$

$$\dot{\rho}_{e_ie_j}=\frac{i}{\hbar}\sum_k\left(V_{e_ig_k}\rho_{g_ke_j}-\rho_{e_ig_k}V_{g_ke_j}\right)-(i\omega_{e_ie_j}+\Gamma)\rho_{e_ie_j}, \tag{2}$$

$$\dot{\rho}_{g_ig_i}=\frac{i}{\hbar}\sum_k\left(V_{g_ie_k}\rho_{e_kg_i}-\rho_{g_ie_k}V_{e_kg_i}\right)-\Gamma_{g_i}\rho_{g_ig_i}+\sum_{j\neq i}\Gamma_{g_jg_i}\rho_{g_jg_j}+(\dot{\rho}_{g_ig_i})_{SE}, \tag{3}$$

$$\dot{\rho}_{g_ig_j}=\frac{i}{\hbar}\sum_k\left(V_{g_ie_k}\rho_{e_kg_j}-\rho_{g_ie_k}V_{e_kg_j}\right)-(i\omega_{g_ig_j}+\Gamma'_{g_ig_j})\rho_{g_ig_j}+(\dot{\rho}_{g_ig_j})_{SE}, \tag{4}$$

where $\omega_{e_ie_j}=\omega_{e_i}-\omega_{e_j}$ and $\omega_{g_ig_j}=\omega_{g_i}-\omega_{g_j}$ denote the Zeeman splitting of excited state and ground states, respectively; $\omega_{k_ik_j}=g_k\mu_bB/\hbar(i=j\pm1)$ is the Raman detuning induced by the magnetic field B, g_k is Lande factor for $k=e$ or g, and μ_b is the Bohr magnetron; $\omega_{e_ig_j}=\omega_{e_i}-\omega_{g_j}$ is transition frequency

between excited and ground degenerate levels. Γ is the total spontaneous emission rate from each excited sublevels. $\Gamma_{e_ig_j}=(\Gamma+\Gamma_{g_j})/2$ is the dephasing rate of the excited-to ground-state coherences, Γ_{g_i} is the total collisional decay rate from sublevel $|g_i\rangle$, $\Gamma_{g_ig_j}$ is the rate of transfer from sublevel $|g_i\rangle\rightarrow|g_j\rangle$, $\Gamma'_{g_ig_j}=(\Gamma_{g_i}+\Gamma_{g_j})/2$ is the dephasing rate of the ground-state coherence. $(\dot{\rho}_{g_ig_j})_{SE}$ is the spontaneous-emission repopulation, which is written as

$$(\dot{\rho}_{g_ig_j})_{SE}=(2F_e+1)\Gamma_{F_e\rightarrow F_g}\sum_{(q,q'=-F_e,+F_e),(p=-1,1)}(-1)^{p-k-q'}\times\begin{pmatrix}F_g & 1 & F_e\\ -k & p & q\end{pmatrix}\rho_{e_qe_{q'}}\begin{pmatrix}F_e & 1 & F_g\\ -q' & -p & k'\end{pmatrix}.$$

The dipole moments of transitions are $\mu_{e_{-1}g_{-2}}=\mu_{e_1g_2}=-\sqrt{\frac{5}{21}}\mu$, $\mu_{e_{-1}g_0}=\mu_{e_1g_0}=-\sqrt{\frac{1}{7}}\mu$, $\mu_{e_0g_{-1}}=\mu_{e_0g_1}=-\sqrt{\frac{1}{14}}\mu$, $\mu_{e_{-1}g_{-1}}=\mu_{e_1g_1}=-\sqrt{\frac{4}{21}}\mu$, and $\mu_{e_0g_0}=-\sqrt{\frac{3}{14}}\mu$ for the Cs atom [40].

$V_{e_ig_j}$ is the interaction energy for the transition $|e_i\rangle\leftrightarrow|g_j\rangle$, and it is directly proportional to Rabi frequency of interacting light. In Fig. 6(a) and Fig. 6(b), the coupling light couples a different transition $|e_i\rangle\leftrightarrow|g_j\rangle$ with $M_{F_e}=i\leftrightarrow M_{F_g}=i$ and $M_{F_e}=i\leftrightarrow M_{F_g}=i\pm1$, respectively, thus the $V_{e_ig_j}$ takes a different from for the different configuration of Fig. 6(a) and Fig. 6(b). In the following, we discuss the quantum coherence for the two cases, respectively.

A. Numerical results for the energy-level scheme shown in Fig. 6(a)

In Fig. 6(a), the coupling light with π polarization is interacting with the transition $|e_i\rangle\leftrightarrow|g_i\rangle$ $(i=0,\pm1,\pm2)$, and meanwhile the probe light with $\sigma_\pm$ polarizations is interacting with the transition $|e_i\rangle\leftrightarrow|g_j\rangle$ $(i=j\pm1, i=0,\pm1,\pm2)$. In this case, when we ignore the effect of spatial amplitude, $V_{e_ig_j}$ are written as $V_{e_ig_j}=\hbar V_{e_ig_j}(\omega_p)e^{-i\omega_pt}$ and $V_{e_ig_j}=\hbar V_{e_ig_j}(\omega_c)e^{-i\omega_ct}$ with $i=0,\pm1,\pm2$, $j=i\pm1$. Here the magnitudes of $2V_{e_ig_j}(\omega_p)=\mu_{e_ig_j}E_p/2^{1/2}\hbar$ and $2V_{e_ig_j}(\omega_c)=\mu_{e_ig_j}E_c/2^{1/2}\hbar$ are defined as the probe and the drive Rabi frequency, respectively. Let $V_{e_ig_j}(\omega_p)$ and $V_{e_ig_j}(\omega_c)$ be real for simplicity.

In order to simplify the calculation, we consider the condition that the coupling light is much stronger than the probe light, thus we treat the coupling field to all orders in its Rabi frequency and meanwhile probe the field to first order. Then $\rho_{e_ig_j}$ oscillates at three frequencies [41,42] the pump frequency ω_c, the probe frequency ω_p, and the four-wave mixing frequency $2\omega_c-\omega_p$. And considering the interaction scheme in Fig. 6(a), we therefore express $\rho_{e_ig_j}$ in terms of its Fourier amplitudes as

$$\rho_{e_ig_j}=\rho_{e_ig_j}(\omega_p)e^{-i\omega_pt}+\rho_{e_ig_j}(2\omega_c-\omega_p)e^{-i(2\omega_c-\omega_p)t} \quad (5)$$

and $\rho_{e_ig_j}$ in terms of its Fourier amplitudes as

$$\rho_{e_ig_i}=\rho_{e_ig_i}(\omega_c)e^{-i\omega_ct}+\rho_{e_ig_i}(2\omega_c-\omega_p)e^{-i(2\omega_c-\omega_p)t}. \quad (6)$$

Similarly, the populations and coherences within the same hyperfine level can be written as

$$\rho_{k_ik_j}=\rho^{dc}_{k_ik_j}+\rho_{k_ik_j}(\omega_c-\omega_p)e^{-i(\omega_c-\omega_p)t}+\rho_{k_ik_j}(\omega_p-\omega_c)e^{-i(\omega_p-\omega_c)t}, \quad (7)$$

where $\rho_{k_ik_j}(\omega_c-\omega_p)e^{-i(\omega_c-\omega_p)t}$ and $\rho_{k_ik_j}(\omega_p-\omega_c)e^{-i(\omega_p-\omega_c)t}$ are population and coherence oscillations at frequencies $\omega_c-\omega_p$ and $\omega_p-\omega_c$.

We solve Eq. (1)–(7) in steady state, for which we set the time derivatives of the Fourier amplitudes equal to zero. The probe absorption is calculated from the imaginary part of the susceptibility $\chi(\omega_p)$; we have

$$\begin{aligned}\mathrm{Im}\,\chi(\omega_p)\propto\mathrm{Im}(\{&\mu_{e_{-2}g_{-3}}[\rho_{e_{-2}g_{-3}}(\omega_p)+\rho_{e_2g_3}(\omega_p)]\\&+\mu_{e_{-2}g_{-1}}[\rho_{e_{-2}g_{-1}}(\omega_p)+\rho_{e_2g_1}(\omega_p)]\\&+\mu_{e_{-1}g_{-2}}[\rho_{e_{-1}g_{-2}}(\omega_p)+\rho_{e_1g_2}(\omega_p)]\\&+\mu_{e_{-1}g_0}[\rho_{e_{-1}g_0}(\omega_p)+\rho_{e_1g_0}(\omega_p)]\\&+\mu_{e_0g_{-1}}[\rho_{e_0g_{-1}}(\omega_p)+\rho_{e_0g_1}(\omega_p)]\}/(V_{e_0g_{-1}}/\gamma_{eg})).\end{aligned} \quad (8)$$

In our calculation, we set the drive field detuning to zero, i.e., $\Delta=\omega_c-\omega_{e_0g_0}=0$; the probe field detuning is $\delta=\omega_p-\omega_{e_0g_0}$. We take $\Gamma'_{g_ig_j}/\Gamma=\Gamma_{g_j}/\Gamma=0.044$, which is based on the fact that the collisional decay rate from sublevels of $|g_i\rangle$, the transfer rate from sublevel $|g_i\rangle\rightarrow|g_j\rangle$, and the dephasing rate of the ground-state coherence are smaller than the decay rate from excited to ground state Γ, for the Cs D_2 line, $\Gamma=5.2$ MHz, i.e., the natural linewidth of Cs D_2 line [40].

When a magnetic field is present, the Zeeman splitting in the excited and ground states occurs simultaneously, the degeneracy of the two-level system is broken. Note that the Zeeman splitting Δe (or $\omega_{e_1e_0}$) of the excited state is not always equal to the splitting Δg (or $\omega_{g_1g_0}$) of the ground state. According to the data of Cs atoms for the hyperfine levels of $6S_{1/2},F_g=3$ and $6P_{3/2},F_e=2$, we take $\Delta e=\mu_B g_F B/\hbar$ $(g_F=2/3)$, $\Delta g=\mu_B g'_F B/\hbar$ $(g'_F=1/4)$. In this case, the total system can be regarded as the superposition of the simple two-level and three-level subsystems, and therefore the quantum coherence show the complex effects resulted from the superposition of simple subsystems. In Fig. 6(a), the system can be treated as the superposition of ten Λ-type $(M_{F_g}=i-1\leftrightarrow M_{F_e}=i\leftrightarrow M_{F_g}=i$ and $M_{F_g}=i+1\leftrightarrow M_{F_e}=i\leftrightarrow M_{F_g}=i)$ and ten V-type $(M_{F_e}=i-1\leftrightarrow M_{F_g}=i\leftrightarrow M_{F_e}=i$ and $M_{F_e}=i+1\leftrightarrow M_{F_g}=i\leftrightarrow M_{F_e}=i)$ simple three-level systems, thus the resulted quantum coherence presents the compositive EIT of several V-type and Λ-type subsystems.

The theoretical absorption spectra of the probe beam as a function of the probe detuning for the different strength of magnetic field B are shown in the left-hand part of Fig. 7. The intensity of the coupling and probe lights are taken to be $V_c/\Gamma=V_{e_ig_i}(\omega_c)/\Gamma=1.138$ $(i=0,\pm1)$, $V_p/\Gamma=V_{e_ig_j}(\omega_p)/\Gamma=0.171$ $(j=i\pm1)$. Consider the real transition of $F_e=2\leftrightarrow F_g=3$, in which there are five coupling fields V_c and ten probe fields V_p interacting with the Zeeman sublevels, thus the total Rabi frequencies of coupling and probe fields (Ω_c and Ω_p) are five and ten times V_c and V_p, respectively ($\Omega_c=5V_c,\Omega_p$

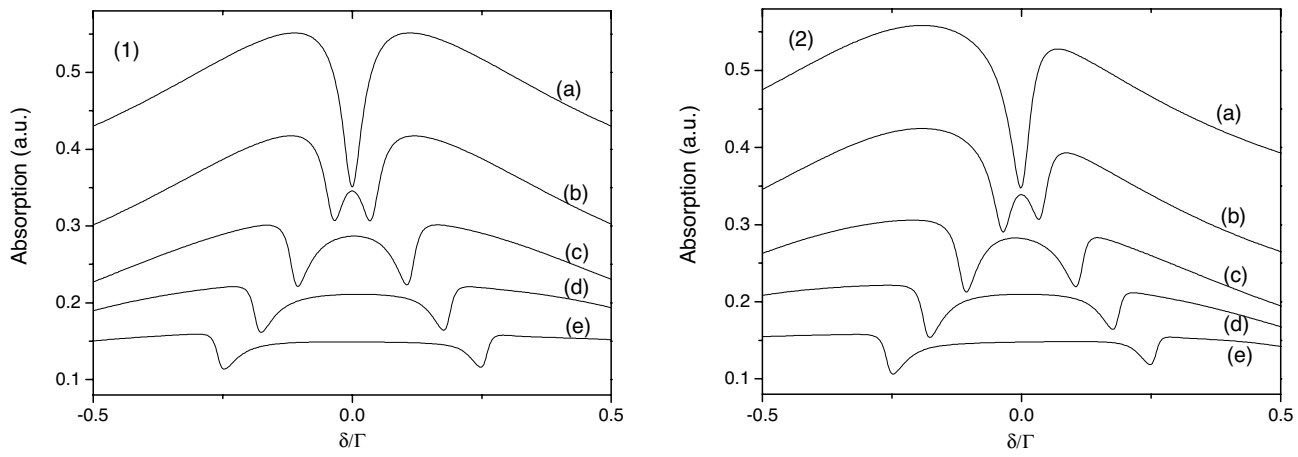

FIG. 7. The theoretical absorption spectra of the probe beam vs probe detuning with different strength of magnetic field B. Left-hand side: $k_{p,c}v=0$; right-hand side: $k_{p,c}v=0.142\Gamma$. The Rabi frequency of the coupling and probe lights are $V_c/\Gamma=1.138$ and $V_p/\Gamma=0.171$. Curve (a), (b), (c), (d), and (e) are for $B=0$, $B=2.8$, $B=8.4$, $B=14$, and $B=19.6$.

$=10V_p$). The left-hand part of Fig. 7(a) is the standard spectrum of EIT when we take $B=0$; As experimentally measured in Fig. 3, when the magnetic field is present, the EIT window is divided into two windows due to the multicoherence induced by the Zeeman multilevel states [Fig. 7(b) with $B=2.8$]; We can see from Figs. 7(c)–7(f) that, by increasing the magnetic field, the two transparency maxima of EIT windows have shifted their position from resonance to off resonance. Comparing the left-hand side of Fig. 7 with Fig. 2, we find qualitative agreement between theoretical and experimental results.

Though it is in qualitative agreement between the numerical and experimental data, when we compare Fig. 2 with the left-hand side of Fig. 7, we still can see the minor difference between these two figures that the numerical calculation shows the symmetric EIT windows, but the two EIT windows in Fig. 2 are asymmetric, which may come from the effect of Doppler broadening. To take the effect into account, we need to consider the experimental scheme in which the drive and probe beams are copropagating and their frequencies are very close, thus an atom moving towards the driven and probe beams with velocity v_z "sees" their frequencies upshifted by an amount $k_{p,c}v_z$; here $k_{p,c}$ is the wave number for the coupling and probe laser, v_z is an averaged velocity averaged over a given velocity distribution $f(v_z)$, which is the Gaussian distribution function of atomic velocities $f(v_z)=(1/v\sqrt{\pi})e^{-v_z^2/v^2}$. Here we give a qualitative analysis by replacing the detuning $\Delta \Rightarrow \Delta+k_cv$ and $\delta \Rightarrow \delta+k_pv$ with $v\propto\sqrt{\langle v_z^2\rangle}$ and $\langle v_z^2\rangle=\int v_z^2 f(v_z)dv_z$, where $v=\sqrt{2k_BT/M}$ is the most probable speed of atoms at a given temperature T, M is the atomic mass, and k_B is the Boltzmann constant [43,44]. In our numerical discussion, we set $k_{p,c}v=0.142\Gamma$, with which the calculated curves (see the right-hand side of Fig. 7) are approximately matched with the experiment results, in which the non-Lorentzian line shapes of EIT windows are observed; thus we can conclude that the main reason for the asymmetrical EIT resonance comes from the effect of Doppler broadening.

When we fix the strength of magnetic field $B=9.8$ and the Rabi frequency of probe beam $V_p/\Gamma=0.171$, it is seen that with the Rabi frequency of coupling light V_c decreasing, both the EIT windows become narrower as shown in the left-hand side of Fig. 8. From curves of 8(a) to curves 8(f), the Rabi frequency is decreased from $V_c/\Gamma=1.138$ to 2.42. The right-hand side of Fig. 8 is the case for the effect of Doppler broadening and is taken to be $k_{p,c}v=0.142\Gamma$. Obviously these effects are in agreement with the experimental data in Fig. 3. From the view point of theory, the physical reason for the broadening EIT linewidth is similar to that of the EIT linewidth in homogeneously broadened medium, where $\Gamma_{EIT}=\Omega^2/\gamma$, when the power of the pump beam is increasing, more and more detuned atoms are pumped into the ground state, i.e., γ increases, on the other hand, when all atoms are pumped, the decay of atoms do not increase anymore, then the broadening of the EIT linewidth is strongly dependent on the intensity of the pump beam.

B. Numerical results for the energy-level scheme shown in Fig. 6(b)

As shown in Fig. 6(b), the transition $F_e=2\leftrightarrow F_g=3$ is driven and probed by both of the two lights having two equal left-handed and right-handed circular polarized components $\sigma_\pm$. Different from the case in Sec. III A, here the interaction energy for the transition from level g_j to e_i is written as $V_{e_ig_j}=\hbar V_{e_ig_j}(\omega_c)e^{-i\omega_c t}+\hbar V_{e_ig_j}(\omega_p)e^{-i\omega_p t}$ with $i=0,\pm1,\pm2, j=i\pm1$. Of course the magnitudes of $2V_{e_ig_j}(\omega_p)=\mu_{e_ig_j}E_p/2^{1/2}\hbar$ and $2V_{e_ig_j}(\omega_c)=\mu_{e_ig_j}E_c/2^{1/2}\hbar$ are the Rabi frequencies of probe and drive fields, respectively. Still considering the condition that the coupling light is much stronger than probe light, we treat the coupling field to all orders in its Rabi frequency and meanwhile probe the field to first order. We therefore express $\rho_{e_ig_j}$ in terms of its Fourier amplitudes as

$$\rho_{e_ig_j}=\rho_{e_ig_j}(\omega_c)e^{-i\omega_c t}+\rho_{e_ig_j}(\omega_p)e^{-i\omega_p t}+\rho_{e_ig_j}(2\omega_c-\omega_p)e^{-i(2\omega_c-\omega_p)t}. \quad (9)$$

Similarly, the populations and coherences within the same hyperfine level can be written as

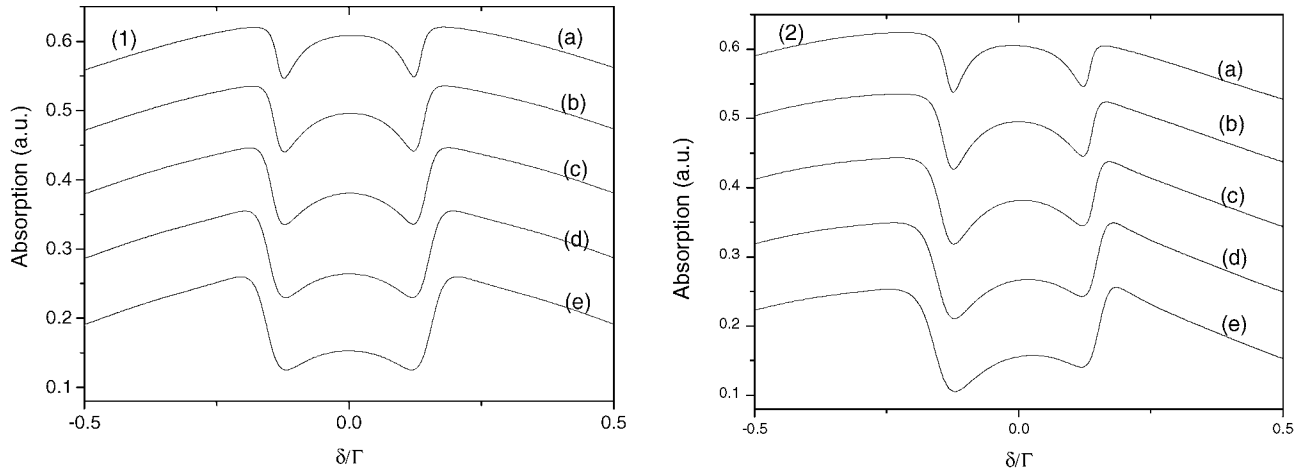

FIG. 8. The theoretical absorption spectra of the probe beam depending on the V_c of the coupling beam with fixed strength of magnetic field $B=9.8$ and probe beam $V_p/\Gamma=0.171$. (1) $k_{p,c}v=0$; (2) $k_{p,c}v=0.142\Gamma$. $V_c/\Gamma=1.138$ in curve (a); $V_c/\Gamma=1.571$ in curve (b); $V_c/\Gamma=1.902$ in curve (c); $V_c/\Gamma=2.21$ in curve (d); $V_c/\Gamma=2.42$ in curve (e).

$$\rho_{k_i k_j} = \rho^{dc}_{k_i k_j} + \rho_{k_i k_j}(\omega_c - \omega_p)e^{-i(\omega_c-\omega_p)t} + \rho_{k_i k_j}(\omega_p - \omega_c)e^{-i(\omega_p-\omega_c)t}, \tag{10}$$

where $\rho_{k_i k_j}(\omega_c-\omega_p)e^{-i(\omega_c-\omega_p)t}$ and $\rho_{k_i k_j}(\omega_p-\omega_c)e^{-i(\omega_p-\omega_c)t}$ are population and coherence oscillations at frequencies $\omega_c-\omega_p$ and $\omega_p-\omega_c$. In the steady state, we obtain a set of linear equations for the Fourier amplitudes, and if the relation $\rho_{ij}(\omega_k)=\rho^*_{ij}(-\omega_k)$ is taken into account, these linear equations are readily solved.

The system shown in Fig. 6(b) can be considered as the superposition of ten pure two-level ($M_{F_g}=i-1\leftrightarrow M_{F_e}=i$ and $M_{F_g}=i+1\leftrightarrow M_{F_e}=i$), ten Λ-type three-level ($M_{F_g}=i-1\leftrightarrow M_{F_e}=i\leftrightarrow M_{F_g}=i+1$, $M_{F_g}=i-1\leftrightarrow M_{F_e}=i\leftrightarrow M_{F_g}=i+1$), and six V-type three-level ($M_{F_e}=i-1\leftrightarrow M_{F_g}=i\leftrightarrow M_{F_g}=i+1$) subsystems, thus the absorption spectrum due to the competition between electromagnetically induced transparency of three-level subsystems and absorption effects of pure two-level systems might has a complex structure. The probe absorption calculated from Eq. (8) is shown in Fig. 9. Figure 9 (left-hand side) is the absorption spectrum without the effect of Doppler broadening ($k_{p,c}v=0$), and in Fig. 9 right-hand side, we set $k_{p,c}v=0.142\Gamma$ when a magnetic field is applied. The degeneracy of the two-level system is broken and the Zeeman splitting in the excited and ground states occurs simultaneously. As measured in Fig. 6, when the intensity of magnetic field B is increased from 0 to 17.6, the one EIT window [Fig. 9(a)] obtained from the quantum coherence of degenerate two-level system is broken up into three transparency peaks [Figs. 9(b)–9(g)]. And it is also shown that the points of the EIT peaks at the right and left sides are shifted its position far from the center of zero detuning of probe light with the magnetic field increasing, and meanwhile the EIT window in the center does not move its position. This effect of shifting points is the result that the Zeeman splitting is increased with the magnetic field increasing, thus the bigger spacing between the two lower levels of

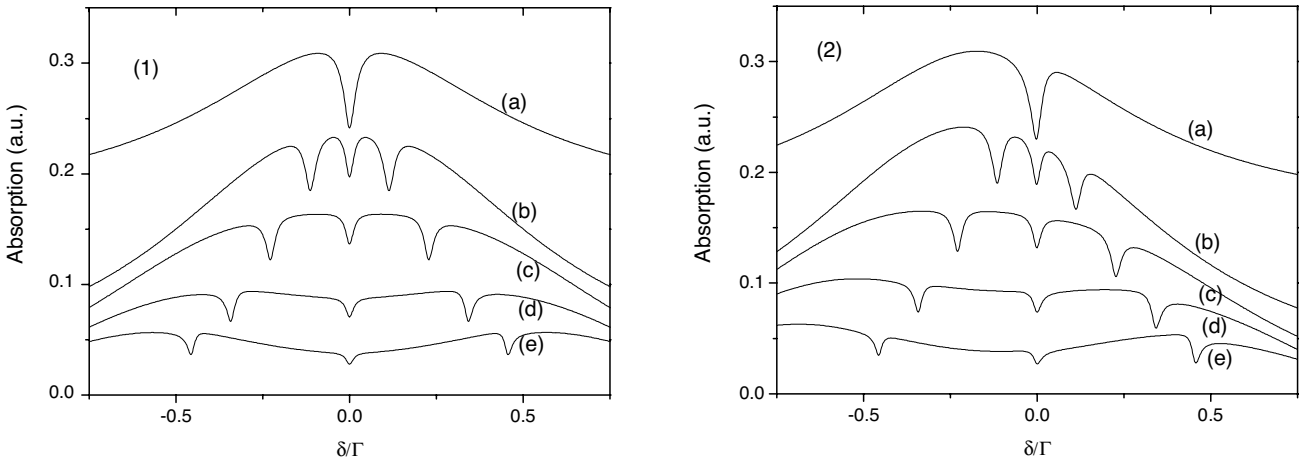

FIG. 9. The absorption spectra of the probe beam vs probe detuning with different strength of magnetic field B. Left-hand side $k_{p,c}v=0$; Right-hand side $k_{p,c}v=0.142\Gamma$. The Rabi frequency of the coupling and probe lights are $V_c/\Gamma=1.138$ and $V_p/\Gamma=0.175$. Curves (a), (b), (c), (d), and (e) are for $B=0$, $B=4.4$, $B=8.8$, $B=13.2$, and $B=17.6$.

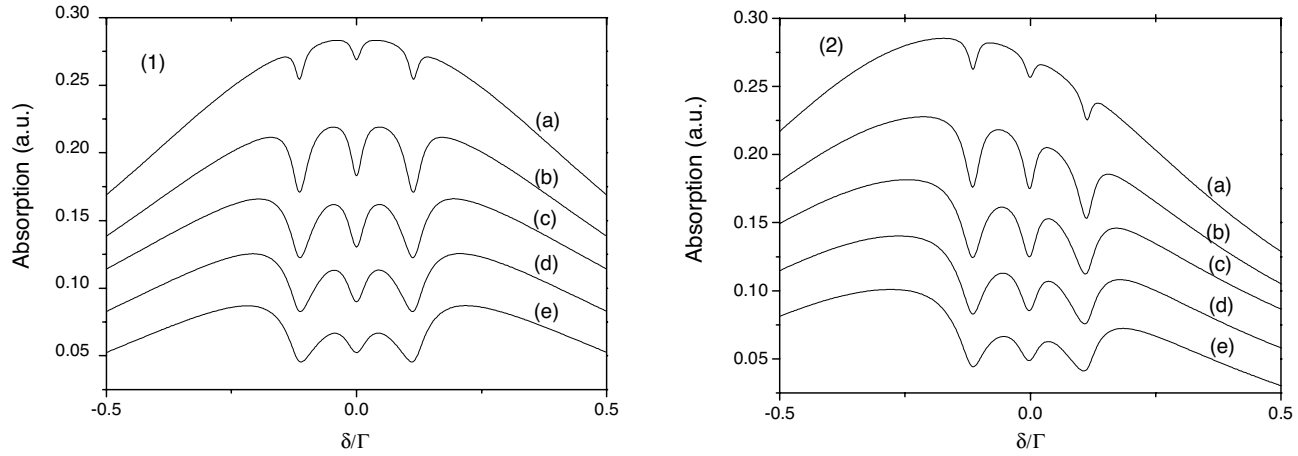

FIG. 10. Theoretical prediction of absorption spectra versus the probe detuning for different V_c. The strength of magnetic field $B=4.4$ and probe beam $V_p/\Gamma=0.175$. (1) $k_{p,c}v=0$; (2) $k_{p,c}v=0.142\Gamma$. $V_c/\Gamma=0.252$ in curve (a); $V_c/\Gamma=0.569$ in curve (b); $V_c/\Gamma=0.831$ in curve (c); $V_c/\Gamma=0.971$ in curve (d); $V_c/\Gamma=1.12$ in curve (e).

Λ-type systems or the two upper level of V-type systems in two-level system leads to the shift of transparency points due to the two-photon resonance of EIT.

In the process of numerical calculation, the Rabi frequencies of coupling and probe beams $[V_{e_ig_j}(\omega_c)$ and $V_{e_ig_j}(\omega_c)]$ represent the frequencies interacted between the Zeeman sublevels, for the real transition of Cs ensemble $F_e=2\leftrightarrow F_g=3$, there are ten parts of coupling fields and ten parts of probe fields interacting with the Zeeman sublevels, thus the total Rabi frequencies of coupling and probe fields (Ω_c and Ω_p, which correspond to the values of experiment) are ten times of $V_{e_ig_j}(\omega_c)$ and $V_{e_ig_j}(\omega_c)$, respectively. It is obviously seen that the curves in Fig. 9 are qualitatively in agreement with the experimental results in Fig. 4. And considering the effect of Doppler broadening in the right-hand side of Fig. 9, the asymmetry of two EIT peaks has accordingly happened.

Then, when we fix the intensity of magnetic field $B=4.4$ and the Rabi frequency of probe beam $V_p/\Gamma=0.175$, respectively, and change the Rabi frequency of coupling beam V_c, it is seen that with the Rabi frequency of coupling light V_c decreased, all the three EIT windows become narrower as shown in Figs. 10(a)–10(e). Figures 10(a), 10(b), 10(c), 10(d), and 10(e) are for the Rabi frequencies of coupling beam $V_c/\Gamma=0.252, 0.569, 0.831, 0.971, 1.12$. These numerical calculations are in line with the experimental results in Figs. 5(a)–5(f). It is shown in Fig. 10 that the distinguishable three EIT peaks are obtained at the mediate power of coupling beam, which is an important condition for the application of multichannel information process.

Notice that the separations among excited hyperfine levels are smaller than the Doppler linewidth at room temperature. In this case, due to the velocity distribution, three different atomic transition, one cycling transition $F_e=2\leftrightarrow F_g=3$, two open transitions $F_g=3\leftrightarrow F_e=3$ and $F_g=3\leftrightarrow F_e=4$, contribute to absorption the signal in each case. Taking into account high intensity and small frequency detuning of coupling beam, the atomic response is quantitatively dominated by the cycling transition $F_e=2\leftrightarrow F_g=3$ because of the efficient optical pumping. Thus the absorption spectra for the real system are qualitative in agreement with the theoretical prediction as discussed in Refs. [10,24].

IV. CONCLUSIONS

In this paper, the quantum coherence in the quasidegenerate two-level system of transition $F_e=2\leftrightarrow F_g=3$ has been experimentally and theoretically discussed. The splitting of EIT window, the shifting and widening of split EIT windows have been investigated in the presence of magnetic field. It has been demonstrated that the quantum coherence is strongly dependent on the combination of the polarization of coupling and probe lights. All these effects are qualitatively explained with the theoretical discussion. The asymmetry of observed spectral has been explained by introducing a laser frequency offset from the optical resonance.

ACKNOWLEDGMENTS

One of the authors (J.Z.) wish to thank Ennio Arimondo and Shi-Yao Zhu for important suggestion. We acknowledge the funding support from NSFC/RGC joint research scheme (Grant Nos. 60518001 and 10674089), from the Program for Changjiang Scholars and Innovative Research Team in University, Shanxi Natural Science Foundation (Grant No. 20041039) and returned Scholar Foundation.

[1] S. E. Harris, J. E. Field, and A. Imamoglu, Phys. Rev. Lett. **64**, 1107 (1990).
[2] K. J. Boller, A. Imamolu, and S. E. Harris, Phys. Rev. Lett. **66**, 2593 (1991).
[3] J. Gea-Banacloche, Y. Q. Li, S. Jin, and M. Xiao, Phys. Rev. A **51**, 576 (1995).
[4] G. Alzetta, L. Moi, and G. Orriols, Nuovo Cimento Soc. Ital. Fis., B **52B**, 209 (1979).
[5] E. Arimondo, Prog. Opt. **35**, 257 (1996).
[6] H. R. Gray, R. M. Whitley, and C. R. Stroud, Opt. Lett. **3**, 218 (1978).
[7] E. Arimondo and G. Orriols, Lett. Nuovo Cimento Soc. Ital. Fis. **17**, 333 (1976).
[8] S. E. Harris, Phys. Rev. Lett. **62**, 1033 (1989).
[9] M. O. Scully, S. Y. Zhu, and A. Gavrielides, Phys. Rev. Lett. **62**, 2813 (1989).
[10] A. M. Akulshin, S. Barreiro, and A. Lezama, Phys. Rev. A **57**, 2996 (1998).
[11] A. V. Taichenachev, A. M. Tumaikin, and V. I. Yudin, Phys. Rev. A **61**, 011802 (1999).
[12] C. Andreeva, S. Cartaleva, Y. Dancheva, V. Biancalana, A. Burchianti, C. Marinelli, E. Mariotti, L. Moi, and K. Nasyrov, Phys. Rev. A **66**, 012502 (2002).
[13] S. K. Kim, H. S. Moon, K. Kim, and J. B. Kim, Phys. Rev. A **68**, 063813 (2003).
[14] M. O. Scully, Phys. Rev. Lett. **67**, 1855 (1991).
[15] H. Lee, M. Fleischhauer, and M. O. Scully, Phys. Rev. A **58**, 2587 (1998).
[16] C. Liu, Z. Dutton, C. H. Behroozi, and L. V. Hau, Nature (London) **409**, 490 (2001).
[17] S. E. Harris and Y. Yamamoto, Phys. Rev. Lett. **81**, 3611 (1998).
[18] Agedi N. Boto, Pieter Kok, Daniel S. Abrams, Samuel L. Braunstein, Colin P. Williams, and Jonathan P. Dowling, Phys. Rev. Lett. **85**, 2733 (2000).
[19] L. V. Hau, S. E. Harris, Z. Dutton, and C. H. Behroozi, Nature (London) **397**, 594 (1999).
[20] L. J. Wang, A. Kuzmich, and A. Dogariu, Nature (London) **406**, 277 (2000).
[21] L. M. Narducci, M. O. Scully, G.-L. Oppo, P. Ru, and J. R. Tredicce, Phys. Rev. A **42**, 1630 (1990).
[22] Yong-qing Li and Min Xiao, Phys. Rev. A **51**, R2703 (1995).
[23] A. Lezama, S. Barreiro, and A. M. Akulshin, Phys. Rev. A **59**, 4732 (1999).
[24] A. Lezama, S. Barreiro, A. Lipsich, and A. M. Akulshin, Phys. Rev. A **61**, 013801 (1999).
[25] A. Lipsich, S. Barreiro, A. M. Akulshin, and A. Lezama, Phys. Rev. A **61**, 053803 (2000).
[26] C. Goren, A. D. Wilson-Gordon, M. Rosenbluh, and H. Friedmann, Phys. Rev. A **67**, 033807 (2003).
[27] S. K. Kim, H. S. Moon, K. Kim, and J. B. Kim, Phys. Rev. A **68**, 063813 (2003).
[28] K. Kim, H. S. Moon, C. Lee, S. K. Kim, and J. B. Kim, Phys. Rev. A **68**, 013810 (2003).
[29] Ying Gu, Qingqing Sun, and Qihuang Gong, Phys. Rev. A **67**, 063809 (2003).
[30] Ying Gu, Qingqing Sun, and Qihuang Gong, J. Phys. B **37**, 1553 (2004).
[31] Qingqing Sun, Ying Gu, and Qihuang Gong, J. Mod. Opt. **51**, 1899 (2004).
[32] A. D. Wilson-Gordon, Phys. Rev. A **48**, 4639 (1993).
[33] E. Kuznetsova, O. Kocharovskaya, P. Hemmer, and M. O. Scully, Phys. Rev. A **66**, 063802 (2002).
[34] Yong-qing Li and Min Xiao, Phys. Rev. A **51**, 4959 (1995).
[35] A. S. Zibrov, A. B. Matsko, O. Kocharovskaya, Y. V. Rostovtsev, G. R. Welch, and M. O. Scully, Phys. Rev. Lett. **88**, 103601 (2002).
[36] C. H. Van der Wal, M. D. Eisaman, A. André, R. L. Walsworth, D. F. Phillips, A. S. Zibrov, and M. D. Lukin, Science **301**, 196 (2003).
[37] A. Raczyński and J. Zaremba, Opt. Commun. **209**, 149 (2002).
[38] A. Joshi and M. Xiao, Phys. Rev. A **71**, 041801 (2005).
[39] F. Renzoni, W. Maichen, L. Windholz, and E. Arimondo, Phys. Rev. A **55**, 3710 (1997).
[40] Daniel A. Steck, available from ⟨http://steck.us/alkalidata⟩.
[41] A. D. Wilson-Gordon and H. Friedmann, Opt. Lett. **8**, 617 (1983).
[42] R. W. Boyd, M. G. Raymer, P. Narum, and D. J. Harter, Phys. Rev. A **24**, 411 (1981).
[43] Ying Wu and Xiaoxue Yang, Phys. Rev. A **71**, 053806 (2005).
[44] C. Y. Ye, Y. V. Rostovtsev, A. S. Zibrov, and Yu. M. Golubev, Opt. Commun. **207**, 227 (2002).